Materials Chemistry and Physics 271 (2021) 124847

Contents lists available at ScienceDirect

Materials Chemistry and Physics

journal homepage: www.elsevier.com/locate/matchemphys

Trimetallic magnetite-Ti-Au nanoparticle formation: A theoretical approach

A.S. Fedorov [a,b,c,*], E.A. Kovaleva [c], A.E. Sokolov [a,b], M.A. Visotin [a,b], C.R. Lin [d], S. G. Ovchinnikov [a,b]

[a] Siberian Federal University, 660041, Krasnoyarsk, Russia
[b] Kirensky Institute of Physics, Federal Research Center KSC SB RAS, 660036, Krasnoyarsk, Russia
[c] Tomsk State University, 634050, Tomsk, Russia
[d] National Pingtung University, Pingtung City, Pingtung County, 90003, Taiwan

HIGHLIGHTS

- Properties of slabs of Fe3O4, Ti and Au layers are investigated by DFT calculations.
- These slabs are simulate the upper layers of core-shell magnetite nanoparticles.
- Specific energies and wettability of Fe3O4–Ti–Au interfaces are calculated.
- It is shown the intermediate thin Ti layer stabilizes this three-layer structure.
- The Ti layer allows obtaining nanoparticles covered with continuous Au coating.

GRAPHICAL ABSTRACT

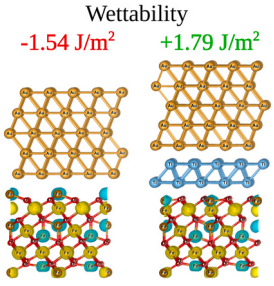

ARTICLE INFO

Keywords:
Magnetite
Gold core-shell nanoparticles
DFT calculations
Interface energy
Nanomedicine

ABSTRACT

Geometric, electronic and magnetic structure of planar slabs consisting of magnetite Fe_3O_4, titanium and gold layers are investigated by DFT-GGA calculations. It is assumed that these slabs can be used to simulate the upper layers of magnetite nanoparticles covered with an intermediate layer of titanium and a gold layer on the surface. Specific energies and spreading parameters (wettability) of the magnetite-gold, magnetite-titanium and titanium-gold interfaces are calculated. The specific energy and spreading parameter of the magnetite-gold interface is found to be negative, while these values of the magnetite-titanium (for thin Ti layer) and magnetite-titan-gold interfaces are significantly positive. This allows us to hope that the intermediate thin layer of titanium at the boundary between the surface of the magnetite nanoparticle and the gold layer stabilizes this three-layer structure and allows obtaining magnetite nanoparticles covered with continuous gold coating.

1. Introduction

At present, due to the progress in various fields of nanotechnology, interest in the production, research and use of nanoparticles with a core-shell structure has greatly increased. Such particles can be used in catalysis, production of magnetic fluids with improved properties [1], etc. Particular attention is paid to the prospect of their utilization in molecular biology and biomedicine, especially in magnetic particle hyperthermia applications. In this area of science fundamentally new revolutionary approaches to diagnosis and treatment have appeared. In

* Corresponding author. Siberian Federal University, 660041, Krasnoyarsk, Russia.
E-mail address: alex99@iph.krasn.ru (A.S. Fedorov).

https://doi.org/10.1016/j.matchemphys.2021.124847
Received 30 December 2020; Received in revised form 17 May 2021; Accepted 14 June 2021
Available online 17 June 2021

1990, the possibility of selecting special oligonucleotides (aptamers) with high affinity for given molecular targets has been demonstrated [2]. Nowadays, the possibility of using complexes based on aptamers and magnetic nanoparticles (NP), in particular, magnetite Fe_3O_4, for magnetic microsurgery have been extensively researched and now appear to be a very promising cancer treatment technology (magnetic-particle-based theranostics) [3]. In accordance with this technology, complexes of magnetic nanoparticles and aptamers attached to their surface, can be moved by adjusting an external magnetic gradient field to the area where cancer cells are present. In this region, the aptamer of the complex attach to the surface of cancer cells, fixing the position of the magnetic nanoparticles. Under the magnetic field varying it is possible to heat the nanoparticle (magnetic particle hyperthermia), and, consequently, the cancer cell, which leads to its death, see Refs. [4,5].

Preparation of magnetite NPs, which have good magnetization, in different conditions have been reported and their properties are well-studied [6–8]. Special attention have been paid to the surface structure and morphology. Zhao et al. have synthesized Fe_3O_4 NPs under a systematic range of conditions using a polyol process, where the crystals obtained ranged shape from cubic, truncated octahedral to octahedral, depending on the pH of solution [7]. While different facets occur, depending on the preparation conditions, e.g. (100), (111), (110), (311), (331), and (511), the two most common facets are the (111) surfaces, which enclose the NP of octahedral morphology, and the (001) plane, added to shape the truncated octahedrons.

One of the simplest ways to reduce the toxicity of the magnetic NPs is to create core-shell nanoparticles having a magnetic core and a biologically inert shell [9,10]. A suitable and optimal material for the formation of the shell is gold, which has good biocompatibility and stability [11]. Due to the formation of a strong sulfur–gold bonds having binding energy of 40 kcal/mol [12], it is easy to functionalize the surface of gold NP with sulfur-containing ligands, thiols and disulfides [13], while the technologies of immobilization of the gold surface with DNA aptamers have been developed. Many reviews have been devoted to this problem [14–18], but all the data presented do not give a clear picture of the continuous coverage of the Fe_3O_4 core with gold, but rather evidence that nanoparticles decorated with gold are obtained [19,20].

In [21] the growth of Au and Pt layers on Fe_3O_4(111) surface by UHV sputtering has been studied for various deposition temperatures and thicknesses. Although the X-ray and TEM analyses show the growth of gold on the Fe_3O_4(111) layer, an absence of solid gold layer was detected even at 750 °C and gold film thickness higher than 7 nm, which are the best conditions for gold layer growth (compared with the other conditions: growth temperatures 200 °C, 400 °C and thickness 3 nm).

It proves the island rather than epitaxial growth mechanism of the gold film on magnetite. It prevents the formation of continuous gold film and confirm the negative value of a magnetite-gold spreading parameter.

Because of the problems above, we suggest using an intermediate titanium layer to cover magnetite NP with a golden layer.

From the known phase diagram, see Fig. 1 it can be seen that titanium and gold form a number of binary compounds with different concentrations of components. This allows us to hope that these metals upon contact will form a solid interface layer with a positive interface energy and the parameter of wettability (spreading parameter) S.

A large number of works devoted to the properties and production of the magnetite-titanium dioxide core-shell nanoparticles [23–30]. The authors of [31] have described polished titanium (Ti) substrates decorated with dispersed gold NP (Au NP/Ti) of various sizes and densities, which effectively catalyze the hydrogen evolution reaction (HER) in 0.5 MH_2SO_4. Composite golden NP/Ti structures were also obtained when anodized Ti foil with a pre-formed periodic structure of holes was used for creating electrochemical biosensors. The foil was covered with a continuous layer of gold first, and then, exposed to high temperature, after which, the gold nanoparticles appeared in the holes [32–34].

Verification of the thermodynamic stability of continuous gold coating of magnetite NPs is the main goal of this article. Since Fe_3O_4 (111) plane is very common and it is the predominant natural cleavage plane, we have chosen to focus on this surface type in our study.

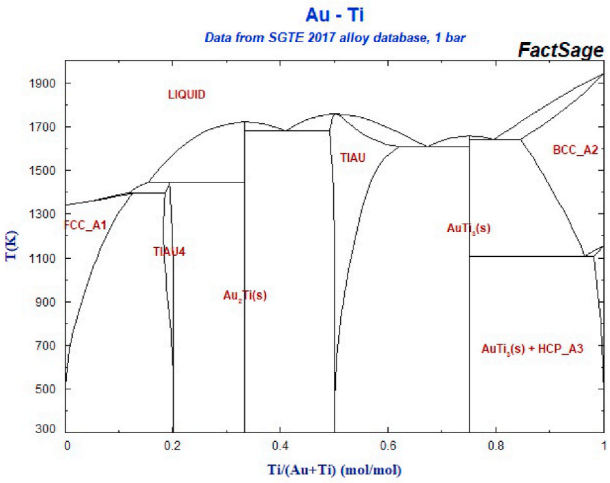

Fig. 1. Ti–Au alloy phase diagram, see [22].

2. Computational details

In this work, calculations of the system geometry, electronic and magnetic properties of single Fe_3O_4, gold, titanium slabs as well as Fe_3O_4/Au and Fe_3O_4/Ti/Au composites were carried out within the density functional theory using the VASP 5.4 code [35,36]. The fully spin-polarized GGA-PBE (Perdew-Becke-Ernzerhof) approximation for exchange-correlation functional [37] and the projector augmented wave [38,39] method (PAW) were used for all calculations. Grimme correction (D3) [40] of weak dispersion interactions was used in order to describe the interaction between slabs correctly. In order to account for the strong correlation effects which are usually significant in transition metal compounds, the simplified form of the LDA + U correction proposed by Dudarev et al. [41] was implemented. The $U = 4.0$ eV parameter for Fe atoms was adopted from earlier calculations of magnetite surfaces [42]. Because of correlation effects are important only for Fe atoms, LDA + U corrections were applied only to these atoms.

Full geometry optimization was performed until the forces acting on atoms became less than 0.05 eV/Å. The energy cut-off was specified as 500 eV in all calculations.

First, the unit cells of bulk Ti, Au and magnetite were optimized, and the translation vectors are found to be in a good agreement with experimental data. Then, Fe_3O_4 (111), Ti (0001) and Au (111) surfaces were constructed by cutting them along the corresponding crystallographic planes. Termination by tetrahedral cites of Fe atoms was chosen for modeling of Fe_3O_4 (111) slab as an energetically favorable according to previous calculations [42–44]. Artificial interactions in periodic boundary conditions were avoided by setting the vacuum interval of 10 Å in direction normal to the interface. The Monkhorst-Pack [45] k-point Brillouin sampling of the first Brillouin zone (1BZ) was used. The k-point grid of 1BZ contained $6 \times 6 \times 6$ and $12 \times 12 \times 12$ points for bulk magnetite and the both metals were used, respectively. $6 \times 6 \times 1$ k-grid was used for all slabs and interfaces.

Fig. 2 and Fig. 3 show optimized geometry and spin density spatial distribution for Fe_3O_4/Au and Fe_3O_4/Ti/Au interfaces respectively. It can be seen that even with thin layers of both metals, their geometric structure practically does not change with respect to the bulk material. However, the positions of the surface oxygen atoms in magnetite are slightly shifted from their initial positions by ~ 0.55 when interacting with Ti.

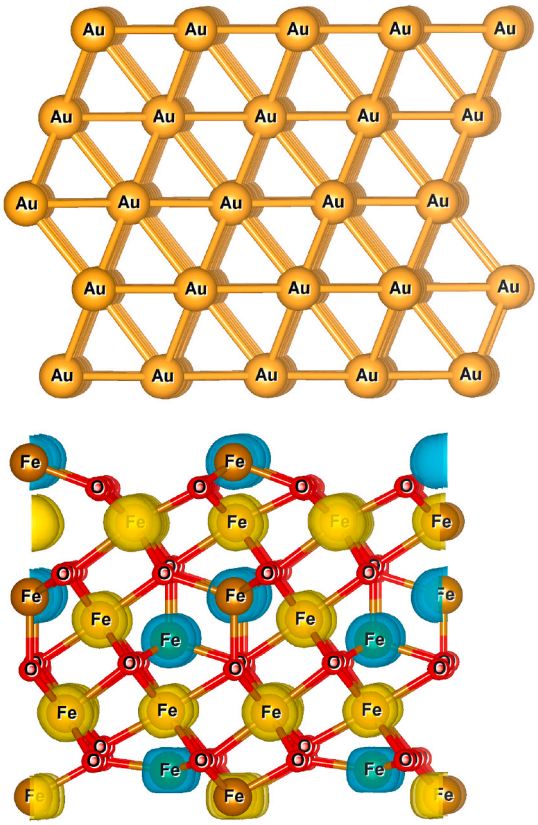

Fig. 2. Example geometry and spin density spatial distribution for Fe_3O_4/Au interface (5 layers of Au). Yellow and blue areas correspond to spin-up and spin-down density, respectively. (For interpretation of the references to colour in this figure legend, the reader is referred to the Web version of this article.)

3. Energies and wettability of (Ti, Au) layers on magnetite surface

First of all, the specific surface energies E_{surf} of single slabs (Fe_3O_4, Ti, Au)) were calculated as follows:

$$E_{surf} = \frac{E_{slab} - E_{bulk} \cdot N_{slab}/N_{bulk}}{2A} \quad (1)$$

where E_{bulk} and E_{slab} correspond to the total energy of bulk and slab examples, respectively. N_{bulk} and N_{slab} correspond to the number of atoms in these. A is the surface area of the slab.

The surface energies of these slabs are given in Table 1.

One can see for correct calculation of the surface energies, it is sufficient to use five layers of titanium or gold only.

In order to investigate bonding of the interfacial region between two slabs (1,2) in the interface, the specific energy of interface $E_{int_{1,2}}$ was calculated as total energy difference between the slabs and the hybrid system taking into account the fact that, when two slabs are connected, two surfaces disappear:

$$A \cdot E_{int_{1,2}} = \sum_{i=1,2} \left(E_{slab_i} - A \cdot E_{surf_i}\right) - E_{hybrid_{1,2}} \quad (2)$$

where $E_{hybrid_{1,2}}$, E_{slab_i} and E_{surf_i} are the total energies of the composite, the slabs and specific surface energies, respectively.

For the case of a three-layer structure the interface energy was calculated quite similarly, where a two-layer hybrid structure $E_{hybrid_{1,2}}$ was chosen as the first slab, to which a third slab was attached:

$$A \cdot E_{int_{12,3}} = E_{hybrid_{1,2}} + E_{slab_3} - A \cdot (E_{surf_2} + E_{surf_3}) - E_{hybrid_{12,3}} \quad (3)$$

To describe the possibility of the formation of a continuous metal layer (titanium, gold) on the surface of a magnetite, as well as on the surface of the magnetite-titanium composite, the spreading parameter S was calculated for all the surfaces. This parameter describe the system total energy change when big liquid metal (Ti, Au) drop spreads over the substrate surface (Fe_3O_4) with forming Fe_3O_4/Me interfaces.

$$S_{1,2} = \frac{E_{slab_1} + E_{bulk_2} \cdot N_{slab_2}/N_{bulk_2} - E_{hybrid_{1,2}}}{A} \quad (4)$$

For complex Fe_3O_4/Ti/Au 3-layer structures notations 1, 2 and 3 correspond to Fe_3O_4 ("bottom layer"), Ti ("intermediate layer") and Au ("wetting layer"). Fe_3O_4/Ti now acts as a new complex substrate, so the

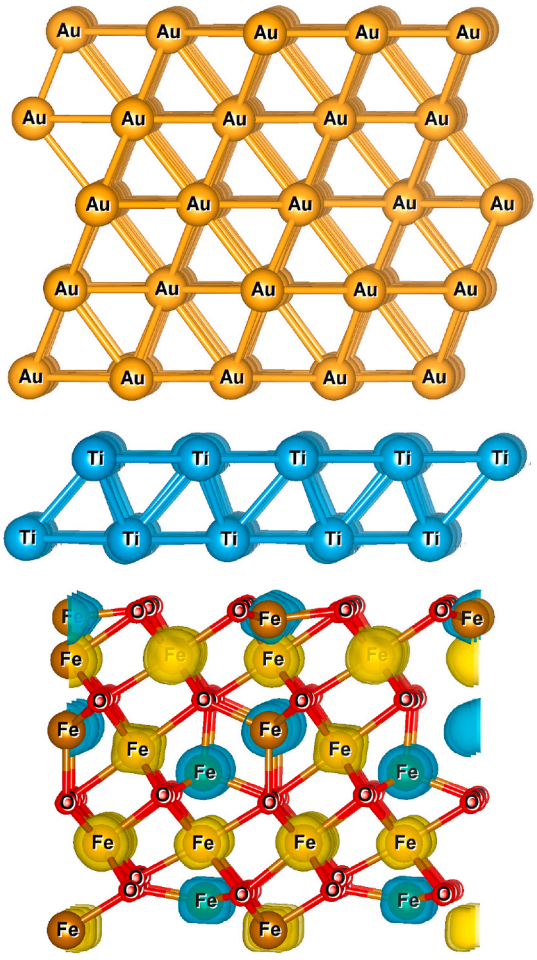

Fig. 3. Example geometry and spin density spatial distribution for Fe_3O_4/Ti/Au interface (2 layers of Ti, 5 layers of Au). Topmost oxygen atoms were displaced by ~ 0.55 Å from their initial positions during the optimization. Yellow and blue areas correspond to spin-up and spin-down density, respectively. (For interpretation of the references to colour in this figure legend, the reader is referred to the Web version of this article.)

Table 1
Dependence of different slab's surface energies E_{surf} on the number of layers N_{layers}.

Slab	N_{layers}	E_{surf}, J./m^2
Fe_3O_4	12	1.13
Ti	2	2.50
Ti	5	2.64
Ti	9	2.61
Au	1	1.00
Au	3	1.41
Au	5	1.40
Au	9	1.43

spreading parameter takes into account Ti surface energy instead of that for Fe_3O_4.

$$S_{2,3} = \frac{E_{hybrid_{1,2}} + E_{bulk_3} \cdot N_{slab_3} / N_{bulk_3} - E_{hybrid_{12,3}}}{A} \quad (5)$$

The specific energies of different interfaces as well as the spreading parameters S are given in Table 2.

One can see that the specific energies of magnetite-gold interface $E_{int_{1,2}}$ as well as the spreading parameter S are negative for all thicknesses of the golden layer.

Positive values of the spreading parameter correspond to the total wetting while its negative value may be attributed to partial or even complete non-wetting. This suggests that the Au/Fe_3O_4 interface is unprofitable, in full agreement with the experimental data, see Introduction. Contrary to that, once Ti is added, the specific interface energies of all magnetite-titanium and magnetite-titanium-gold structures are positive. The spreading parameters S of these structures are positive also, except for magnetite-titanium structures with quite thick Ti layer. It means the gold will spread over the magnetite covered with a thin layer of titanium, and will not aggregate into drops.

4. Electronic and magnetic properties of (Ti, Au) layers on magnetite surface

To investigate (Ti, Au) layer influence on the electronic and magnetic properties of the magnetite slab, the electronic partial density of states (PDOS) of every layer in the complex Fe_3O_4(12 layers)/Ti(2 layers/Au(9 layers) structure were calculated, see Fig. 4 and Fig. 5. In Fig. 4 the contributions from iron (red solid lines), oxygen (black solid lines), titanium (blue dashed lines) and gold (green dotted lines) atoms are shown from bottom to up. Because of similar contributions of gold layers, the contributions of only three bottom Au layers are shown. One can see the contributions of titanium and gold layers prevail near the Fermi level.

Values of total magnetization for all investigated structures are summarized in Table 2. First of all, the total magnetization of pristine 12-layer magnetite slab unit cell turned out to be 19.9, in good agreement with previous results [46]. According to Table 2, the total magnetization doesn't change much for all Fe_3O_4/Me structures, which can indirectly indicate that magnetic properties are preserved in the core-shell nanoparticles with a magnetite core.

Composites spin density spatial distribution is shown in Fig. 2 and Fig. 3. It is clearly seen that iron atoms in different crystal positions have spin densities of opposite signs while Ti and Au layers are non-magnetic.

Table 3 shows the magnetic moments of Fe atoms of different Fe_3O_4/Me structures. These Fe atoms lie in the topmost tetrahedral and different octahedral(1,2) layers. One can see the tetrahedral Fe atoms have significantly lower magnetic moments of opposite sign than the

Table 2
Energy and structural characteristics of the interfaces. d_{Fe-M} reflects the shortest distance between topmost Fe atom and the metal atom from Ti or Au slab. d_{Ti-Au} corresponds to the average distance between atoms of topmost Ti layer and the corresponding Au layer in contact.

Interface	E_{int}, J/m^2	S, J/m^2	d_{Fe-M}, Å	d_{Ti-Au}, Å	magnetization
Fe_3O_4/1Au	−0.92	−0.70	2.72	–	18.50
Fe_3O_4/3Au	−1.32	−1.49	2.78	–	18.61
Fe_3O_4/5Au	−1.40	−1.54	2.77	–	18.41
Fe_3O_4/9Au	−1.47	−1.63	2.59	–	18.86
Fe_3O_4/2Ti	1.23	0.13	2.73		17.62
Fe_3O_4/2Ti/1Au	0.75	2.08	2.72	2.73	17.92
Fe_3O_4/2Ti/3Au	0.88	1.82	2.73	2.74	18.00
Fe_3O_4/2Ti/5Au	0.82	1.79	2.75	2.74	17.87
Fe_3O_4/2Ti/9Au	0.80	1.74	2.73	2.73	17.91
Fe_3O_4/5Ti	1.06	−0.19	2.68	–	17.82
Fe_3O_4/5Ti/5Au	0.61	1.71	2.68	2.72	17.99
Fe_3O_4/9Ti	0.65	−0.61	2.68	2.72	17.99

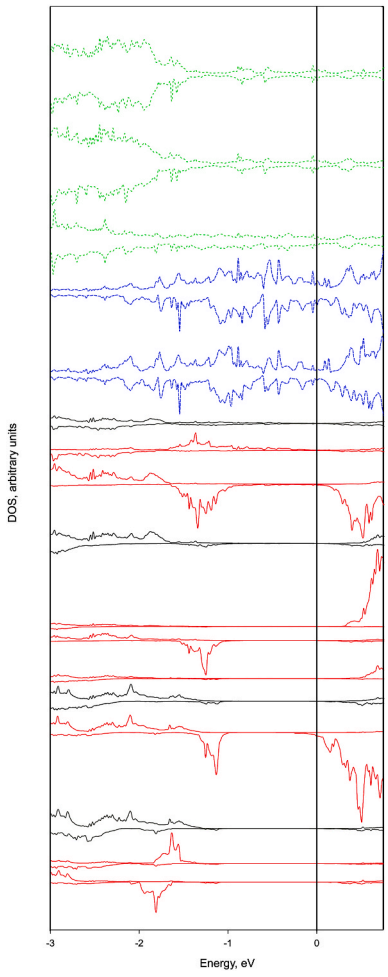

Fig. 4. Partial DOS of every layer in Fe_3O_4/2Ti/9Au complex structure. Green, blue, red and black lines correspond to Au, Ti , Fe and oxygen atoms PDOS. Vertical black line corresponds to the Fermi level. (For interpretation of the references to colour in this figure legend, the reader is referred to the Web version of this article.)

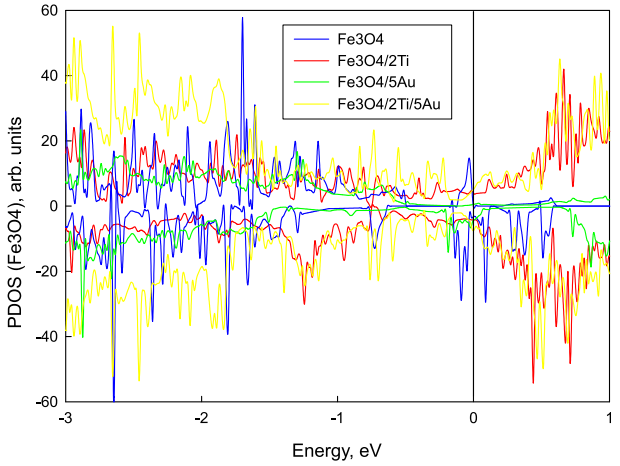

Fig. 5. PDOS for magnetite in Fe_3O_4, Fe_3O_4/5Au (a), Fe_3O_4/2Ti and Fe_3O_4/2Ti/5Au (b) structures. Vertical black line corresponds to the Fermi level.

Table 3
Magnetic moments on the topmost tetrahedral and octahedral Fe atoms.

Interface	Fe_{tet}	Fe_{oct}	Fe_{oct_2}
Fe_3O_4	−3.57	4.21	4.20
Fe_3O_4/5Au	−3.96	4.20	4.21
Fe_3O_4/5Ti	−3.27	3.70	4.16
Fe_3O_4/5Ti/5Au	−3.27	3.70	4.16

atoms in the octahedral positions.

5. Conclusion

By GGA-DFT calculations we have investigated the total energy, geometric and electronic structures of magnetite Fe_3O_4, gold and titanium thin planar slabs as well as their combinations.

We propose that this slab model can be used to simulate the upper layers of magnetite nanoparticles covered with an intermediate layer of titanium and a gold layer on the surface. Based on the analysis of bulk and slab total energies of magnetite, titanium and gold isolated layers, as well as their two-layer and three-layer slabs, the specific energies of interfaces and spreading parameters at the magnetite-gold, magnetite-titanium and titanium-gold boundaries have been calculated. These values are important for understanding the possibility of formation of a thermodynamically stable epitaxial layer of one material on another.

The specific energy of the magnetite-gold interface is found to be negative while these energies of the magnetite-titanium and and the magnetite-titan-gold interfaces are positive.

Similarly, the spreading parameter of the magnetite-gold interface is negative, while those of the magnetite-titanium (except case of thick (5,9) Ti layers), and magnetite-titan-gold interfaces are significantly positive.

Our finding allows us to hope that the intermediate layer of titanium between the magnetite nanoparticle and the gold layer may stabilize this three-layer structure. It indicates a way to obtain stable magnetite nanoparticles covered with solid gold. Inert magnetic core-shell nanoparticles are very promising for applications in nanomedicine, particularly, in magnetic particle hyper-thermia

Electronic and magnetic properties of Fe_3O_4, titanium and gold periodical slabs have been investigated as well. Analyzing the partial density of electronic states (PDOS), we conclude that the magnetite-titanium-gold sandwich is conductive due to the gold layer, while no significant changes were found in the magnetic moments of iron atoms in a magnetite layer.

Thus, our work suggests that it is possible to obtain magnetic nanoparticles of magnetite coated with a continuous layer of gold by using a buffer layer of titanium.

CRediT authorship contribution statement

A.S. Fedorov: Conceptualization, Methodology. **E.A. Kovaleva:** Calculations. **A.E. Sokolov:** Resources, Writing – original draft. **M.A. Visotin:** Validation. **C.R. Lin:** Formal analysis, Visualization. **S.G. Ovchinnikov:** Writing – review & editing.

Declaration of competing interest

The authors declare that they have no known competing financial interests or personal relationships that could have appeared to influence the work reported in this paper.

Acknowledgments

The reported study was funded by Joint Research Project of Russian Foundation for Basic Research # 19-52-52002 and Ministry of Science and Technology, Taiwan MOST # 109-2112-M-153-003 and # 108-2923-M-153-001-MY3.

References

[1] M. Yu, X. Bian, T. Wang, J. Wang, Metal-based magnetic fluids with core-shell structure FeB@SiO2 amorphous particles, Soft Matter 13 (2017) 6340–6348.
[2] A.D. Ellington, J.W. Szostak, In vitro selection of rna molecules that bind specific ligands, nature 346 (1990) 818–822.
[3] I.V. Belyanina, T.N. Zamay, G.S. Zamay, S.S. Zamay, O.S. Kolovskaya, T. I. Ivanchenko, V.V. Denisenko, A.K. Kirichenko, Y.E. Glazyrin, I.V. Garanzha, et al., In vivo cancer cells elimination guided by aptamer-functionalized gold-coated magnetic nanoparticles and controlled with low frequency alternating magnetic field, Theranostics 7 (2017) 3326.
[4] A. Hervault, N.T.K. Thanh, Magnetic nanoparticle-based therapeutic agents for thermo-chemotherapy treatment of cancer, Nanoscale 6 (2014) 11553–11573.
[5] M.V. Efremova, Y.A. Nalench, E. Myrovali, A.S. Garanina, I.S. Grebennikov, P. K. Gifer, M.A. Abakumov, M. Spasova, M. Angelakeris, A.G. Savchenko, M. Farle, N.L. Klyachko, A.G. Majouga, U. Wiedwald, Size-selected Fe3O4-Au hybrid nanoparticles for improved magnetism-based theranostics, Beilstein J. Nanotechnol. 9 (2018"natexlaba) 2684–2699.
[6] X. Yu, Y. Li, Y.W. Li, J. Wang, H. Jiao, DFT+U study of molecular and dissociative Water adsorptions on the Fe 3O4(110) surface, J. Phys. Chem. C 117 (2013) 7648–7655.
[7] L. Zhao, H. Zhang, Y. Xing, S. Song, S. Yu, W. Shi, X. Guo, J. Yang, Y. Lei, F. Cao, Morphology-controlled synthesis of magnetites with nanoporous structures and excellent magnetic properties, Chem. Mater. 20 (2008) 198–204.
[8] J. Sato, M. Kobayashi, H. Kato, T. Miyazaki, M. Kakihana, Hydrothermal synthesis of magnetite particles with uncommon crystal facets, J. Asian. Ceramic.Soc. 2 (2014) 258–262.
[9] K. Chatterjee, S. Sarkar, K.J. Rao, S. Paria, Core/shell nanoparticles in biomedical applications, Adv. Colloid Interface Sci. 209 (2014) 8–39.
[10] Y. Li, J. Liu, Y. Zhong, J. Zhang, Z. Wang, L. Wang, Y. An, M. Lin, Z. Gao, D. Zhang, Biocompatibility of fe3o4@ au composite magnetic nanoparticles in vitro and in vivo, Int. J. Nanomed. 6 (2011) 2805.
[11] J. Fan, W. Hung, W. Li, J. Yeh, Biocompatibility study of gold nanoparticles to human cells, in: 13th International Conference on Biomedical Engineering, Springer, 2009, pp. 870–873.
[12] P.M. Tiwari, K. Vig, V.A. Dennis, S.R. Singh, Functionalized gold nanoparticles and their biomedical applications, Nanomaterials 1 (2011) 31–63.
[13] C.D. Bain, H.A. Biebuyck, G.M. Whitesides, Comparison of self-assembled monolayers on gold: coadsorption of thiols and disulfides, Langmuir 5 (723–727) (1989) 252.
[14] J. Wang, X. Zeng, "Core–shell magnetic nanoclusters, in: J.P. Liu, E. Fullerton, O. Gutfleisch, D. Sellmyer (Eds.), In "Nanoscale Magnetic Materials and Applications, Springer US, Boston, MA, 2009, pp. 35–65.
[15] K.D. Gilroy, A. Ruditskiy, H.-C. Peng, D. Qin, Y. Xia, Bimetallic nanocrystals: syntheses, properties, and applications, Chem. Rev. 116 (2016) 10414–10472.
[16] M.P. Melancon, C. Li, Core-shell magnetic nanomaterials in medical diagnosis and therapy. nanotechnologies for the life sciences, Wiley Online Library, 2011, pp. 259–290, https://doi.org/10.1002/9783527610419.ntls0169.
[17] S.V. Salihov, Y.A. Ivanenkov, S.P. Krechetov, M.S. Veselov, N.V. Sviridenkova, A. G. Savchenko, N.L. Klyachko, Y.I. Golovin, N.V. Chufarova, E.K. Beloglazkina, et al., Recent advances in the synthesis of fe3o4@ au core/shell nanoparticles, J. Magn. Magn Mater. 394 (2015) 173–178.
[18] M.V. Efremova, V.A. Naumenko, M. Spasova, A.S. Garanina, M.A. Abakumov, A. D. Blokhina, P.A. Melnikov, A.O. Prelovskaya, M. Heidelmann, Z.-A. Li, et al., Magnetite-gold nanohybrids as ideal all-in-one platforms for theranostics, Sci. Rep. 8 (2018) 1–19.
[19] H. Maleki, A. Simchi, M. Imani, B. Costa, Size-controlled synthesis of superparamagnetic iron oxide nanoparticles and their surface coating by gold for biomedical applications, J. Magn. Magn Mater. 324 (2012) 3997–4005.
[20] E.A. Kwizera, E. Chaffin, X. Shen, J. Chen, Q. Zou, Z. Wu, Z. Gai, S. Bhana, R. O'Connor, L. Wang, et al., "Size-and shape-controlled synthesis and properties of magnetic–plasmonic core–shell nanoparticles, J. Phys. Chem. C 120 (2016) 10530–10546.
[21] C. Gatel, E. Snoeck, Epitaxial growth of Au and Pt on Fe3O4(1 1 1) surface, Surf. Sci. 601 (2007) 1031–1039.
[22] Thermochemical databases - SGTE - scientific group thermodata europe. https://www.sgte.net/en/thermochemical-databases, 2020-08-01.
[23] J.H. Wei, C.J. Leng, X.Z. Zhang, W.H. Li, Z.Y. Liu, J. Shi, Synthesis and magnetorheological effect of Fe 3 O 4 -TiO 2 nanocomposite, J. Phys. Conf. 149 (2009), 012083.
[24] K.F. Ya, Z. Peng, Z.H. Liao, J.J. Chen, Preparation and photocatalytic property of Ti0 2-Fe 30 4 core-shell nanoparticles, J. Nanosci. Nanotechnol. 9 (2009) 1458–1461.
[25] W.J. Chen, Y.C. Chen, Fe3O4/TiO2 core/shell magnetic nanoparticle-based photokilling of pathogenic bacteria, Nanomedicine 5 (2010) 1585–1593.
[26] M. Stefan, O. Pana, C. Leostean, C. Bele, D. Silipas, M. Senila, E. Gautron, Synthesis and characterization of Fe3O4-TiO2core-shell nanoparticles, J. Appl. Phys. 116 (2014), https://doi.org/10.1063/1.4896070.
[27] S. Khashan, S. Dagher, N. Tit, A. Alazzam, I. Obaidat, Novel method for synthesis of Fe3O4@TiO2 core/shell nanoparticles, Surf. Coating. Technol. 322 (2017) 92–98.
[28] K. Li, S. Liu, Y. Xue, L. Zhang, Y. Han, A superparamagnetic Fe3O4-TiO2 composite coating on titanium by micro-arc oxidation for percutaneous implants, J. Mater. Chem. B 7 (2019) 5265–5276.

[29] S. Khammar, N. Bahramifar, H. Younesi, Preparation and surface engineering of CM-β-CD functionalized Fe3O4@TiO2 nanoparticles for photocatalytic degradation of polychlorinated biphenyls (PCBs) from transformer oil, J. Hazard Mater. 394 (2020) 122422.
[30] C.T. Chen, Y.C. Chen, Fe3O4/TiO2 core/shell nanoparticles as affinity probes for the analysis of phosphopeptides using TiO2 surface-assisted laser desorption/ionization mass spectrometry, Anal. Chem. 77 (2005) 5912–5919.
[31] M.A. Amin, S.A. Fadlallah, G.S. Alosaimi, F. Kandemirli, M. Saracoglu, S. Szunerits, R. Boukherroub, Cathodic activation of titanium-supported gold nanoparticles: an efficient and stable electrocatalyst for the hydrogen evolution reaction, Int. J. Hydrogen Energy 41 (2016) 6326–6341.
[32] K. Grochowska, K. Siuzdak, M. Sokołowski, J. Karczewski, M. Szkoda, G. Śliwiński, Properties of ordered titanium templates covered with Au thin films for SERS applications, Appl. Surf. Sci. 388 (2016) 716–722.
[33] K. Grochowska, M. Szkoda, J. Karczewski, G. Śliwiński, K. Siuzdak, "Ordered titanium templates functionalized by gold films for biosensing applications – towards non-enzymatic glucose detection, Talanta 166 (2017) 207–214.
[34] K. Siuzdak, D. Döhler, J. Bachmann, J. Karczewski, K. Grochowska, Light-improved glucose sensing on ordered Au-Ti heterostructure, Optik 206 (2020) 164166.
[35] G. Kresse, J. Furthmüller, Efficiency of ab-initio total energy calculations for metals and semiconductors using a plane-wave basis set, Comput. Mater. Sci. 6 (1996) 15–50.
[36] G. Kresse, J. Furthmüller, Efficient iterative schemes for ab initio total-energy calculations using a plane-wave basis set, Phys. Rev. B Condens. Matter 54 (1996) 11169–11186.
[37] J.P. Perdew, K. Burke, M. Ernzerhof, Generalized gradient approximation made simple, Phys. Rev. Lett. 77 (1996) 3865–3868.
[38] P.E. Blöchl, Projector augmented-wave method, Phys. Rev. B 50 (1994) 17953–17979.
[39] D. Joubert, From ultrasoft pseudopotentials to the projector augmented-wave method, Phys. Rev. B Condens. Matter 59 (1999) 1758–1775.
[40] S. Grimme, J. Antony, S. Ehrlich, H. Krieg, A consistent and accurate ab initio parametrization of density functional dispersion correction (DFT-D) for the 94 elements H-Pu, J. Chem. Phys. 132 (2010) 154104.
[41] S. Dudarev, G. Botton, Electron-energy-loss spectra and the structural stability of nickel oxide: an LSDA+U study, Phys. Rev. B Condens. Matter 57 (1998) 1505–1509.
[42] J. Noh, O.I. Osman, S.G. Aziz, P. Winget, J.L. Brédas, Magnetite Fe3O4 (111) surfaces: impact of defects on structure, stability, and electronic properties, Chem. Mater. 27 (2015) 5856–5867.
[43] T. Pabisiak, M.J. Winiarski, T. Ossowski, A. Kiejna, Adsorption of gold subnano-structures on a magnetite(111) surface and their interaction with CO, Phys. Chem. Chem. Phys. 18 (2016) 18169–18179.
[44] A. Kiejna, T. Pabisiak, Effect of substrate relaxation on adsorption energies: the example of α-Fe2O3(0001) and Fe3O4(111), Surf. Sci. 679 (2019) 225–229.
[45] H.J. Monkhorst, J.D. Pack, Special points for Brillouin-zone integrations, Phys. Rev. B 13 (1976) 5188–5192.
[46] X. Yu, C.-F. Huo, Y.-W. Li, J. Wang, H. Jiao, Fe3o4 surface electronic structures and stability from gga+ u, Surf. Sci. 606 (2012) 872–879.